

Experimental report

29/08/2022

Proposal: 5-24-675

Council: 4/2021

Title: Role of the crystal structure and oxygen vacancies in the transport properties and electrochemical performance of LaNi_{0.6}Fe_{0.4-x}M_xO_{3- δ}

Research area: Materials

This proposal is a new proposal

Main proposer: Jesus PRADO GONJAL

Experimental team:

Local contacts: Maria Teresa FERNANDEZ DIAZ

Samples: LaNi_{0.6}Fe_{0.3}Cu_{0.1}O_{3- δ}

LaNi_{0.6}Fe_{0.2}Cu_{0.2}O_{3- δ}

LaNi_{0.6}Fe_{0.3}Cr_{0.1}O_{3- δ}

Instrument	Requested days	Allocated days	From	To
D2B	3	3	08/10/2021	11/10/2021

Abstract:

We have investigated LaNi_{0.6}Fe_{0.4-x}M_xO_{3- δ} (M= Cu, Cr) oxides as contact materials for the Reversible Solid Oxide Fuel Cells (RSOFCs) stacks. As B-site dopants influence the crystal structure and electrical properties, the goals of this neutron thermodiffraction proposal are: i) To determine the thermal evolution of the crystal structure of LaNi_{0.6}Fe_{0.3}Cu_{0.1}O_{3- δ} , LaNi_{0.6}Fe_{0.2}Cu_{0.2}O_{3- δ} , and LaNi_{0.6}Fe_{0.3}Cr_{0.1}O_{3- δ} samples at the working conditions of a RSOFC. We will pay special attention to the oxygen vacancies concentration, the orthorhombic δ rhombohedral structural transition and the possible cation and anion structural ordering; ii) To correlate the effect of the crystal structure on the transport and electrochemical properties of the selected materials. For these tasks we ask for 3 days at D2B diffractometer.

Role of the crystal structure and oxygen vacancies in the transport properties and electrochemical performance of $\text{LaNi}_{0.6}\text{Fe}_{0.4-x}\text{M}_x\text{O}_{3-\delta}$

Room temperature NPD patterns for $\text{LaNi}_{0.6}\text{Fe}_{0.2}\text{Cu}_{0.2}\text{O}_{3-\delta}$ and $\text{LaNi}_{0.6}\text{Fe}_{0.3}\text{Cr}_{0.1}\text{O}_{3-\delta}$ samples are shown in Figure 1. These two compounds' structures were refined in the rhombohedral $R-3c$ (#167) space group, which is formed by the perovskite's anti-phase three tilt scheme $a^-a^-a^-$ of the perovskite [1]. Figure 2 shows a representation of the rhombohedral perovskite's crystal structure. The large size of La^{3+} for the A site causes the slightly deformed rhombohedral structure, similar to $\text{LaNiO}_{3-\delta}$, therefore the perovskite is generated by a displacement of O^{2-} from their model position in the cubic perovskite [2,3]. The ideal AO₁₂ cuboctahedron in ABO_3 , which has 12 equal A-O distances, is thus changed into a polyhedron with 3 A-O short-bonds, 6 medium-bonds, and 3 long-bonds. In the case of the BO₆ octahedra, B-O distances are the same. However, the O-B-O angles for the BO₆ octahedron are slightly off from 90°, but the B-O distances are the same. The 8 short A-B lengths are changed to two shorter and six longer, while the A-A and B-B distances remain equal.

La atoms occupy the $6a$ (0, 0, 1/4) Wyckoff sites in the prepared compositions, while Ni, Fe, and Cu/Cr are randomly dispersed at the $6b$ (0, 0, 0) site and O is situated at the $18e$ (x , 0, 1/4) Wyckoff location. The crystallographic formulae of $\text{LaNi}_{0.59(2)}\text{Fe}_{0.20(3)}\text{Cu}_{0.20(3)}\text{O}_{2.87(1)}$ and $\text{LaNi}_{0.63(2)}\text{Fe}_{0.27(2)}\text{Cr}_{0.10(1)}\text{O}_{2.96(1)}$ (at room temperature) were obtained by refining the atomic site occupancies.. Table 1 and Table 2 summarize the unit-cell parameters, atomic positions, isotropic displacement parameters for metal and O atoms, agreement factors and main interatomic distances, after the Rietveld refinement of the crystal structure at room temperature, 400, 700 and 900 °C (figure 3 and figure 4). The neutron powder diffractograms show no extra reflections, indicating that there is no evidence of a superstructure resulting from a potential ordering of the oxygen vacancies or metal cations. The amount of oxygen vacancies increases somewhat for both phases when the samples are heated, resulting in compositions of $\text{LaNi}_{0.59}\text{Fe}_{0.20}\text{Cu}_{0.20}\text{O}_{2.71(1)}$ and $\text{LaNi}_{0.63}\text{Fe}_{0.27}\text{Cr}_{0.10}\text{O}_{2.90(1)}$ at 900 °C.

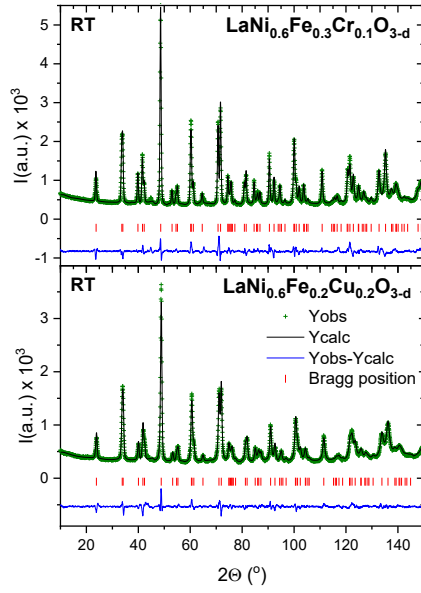


Figure 1. Observed (green crosses), calculated (black, full line), and difference (blue line) neutron powder diffraction profile for $\text{LaNi}_{0.6}\text{Fe}_{0.2}\text{Cu}_{0.2}\text{O}_{3-\delta}$ and $\text{LaNi}_{0.6}\text{Fe}_{0.3}\text{Cr}_{0.1}\text{O}_{3-\delta}$ perovskites. The vertical red bars correspond to the allowed Bragg reflections.

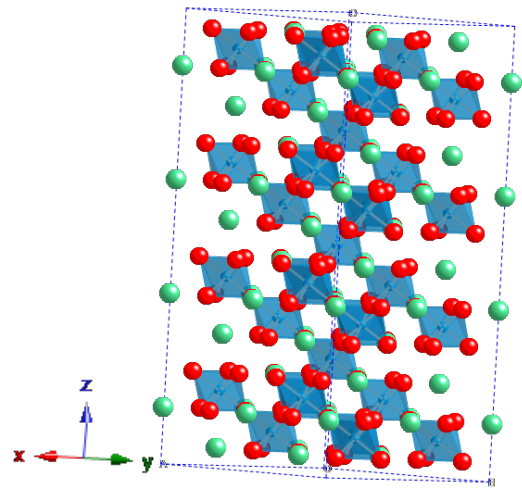


Figure 2. View of the crystal structure, emphasizing BO_6 octahedra (blue). Green spheres indicate La atoms while red spheres show O atoms.

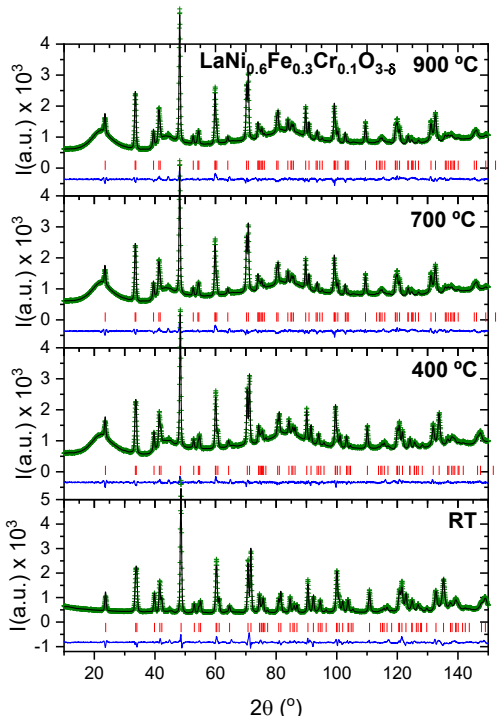


Figure 3. Neutron powder thermodiffraction profiles in air for $\text{LaNi}_{0.6}\text{Fe}_{0.3}\text{Cr}_{0.1}\text{O}_{3-\delta}$

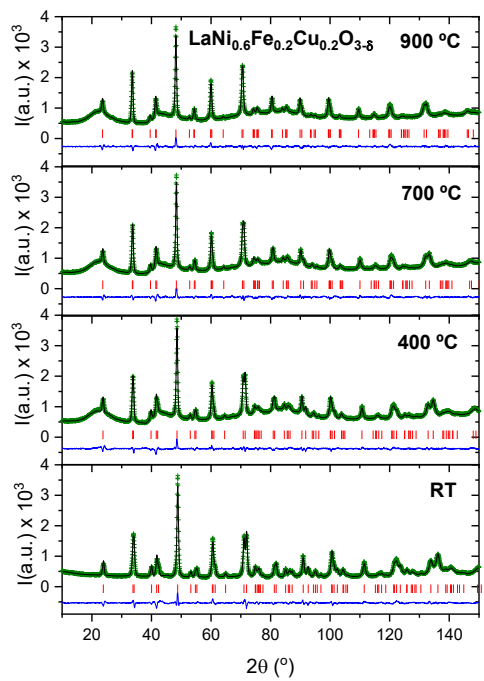


Figure 4. Neutron powder thermodiffraction profiles in air for $\text{LaNi}_{0.6}\text{Fe}_{0.2}\text{Cu}_{0.2}\text{O}_{3-\delta}$.

Table 1. Refined structural parameters obtained from NPD for $\text{LaNi}_{0.6}\text{Fe}_{0.2}\text{Cu}_{0.2}\text{O}_{3-\delta}$ from room temperature to 900 °C. Space group: $R\bar{3}c$

T (°C)	RT	400	700	900
a (Å)	5.4850 (2)	5.5030 (2)	5.5185 (3)	5.5296 (2)
b (Å)	5.4850 (2)	5.5030 (2)	5.5185 (3)	5.5296 (2)
c (Å)	13.2243 (6)	13.3176 (7)	13.4005 (8)	13.4654 (8)
La				
x	0	0	0	0
y	0	0	0	0
z	0.25	0.25	0.25	0.25
Occ.	1	1	1	1
B _{iso} (Å ²)	0.29(2)	0.95(3)	1.39(4)	2.11(2)
Ni/Fe/Cu				
x	0	0	0	0
y	0	0	0	0
z	0	0	0	0
Occ.	0.59(2)/0.20(3)/0.20(3)	0.59/0.20/0.20	0.59/0.20/0.20	0.59/0.20/0.20
B _{iso} (Å ²)	0.10(1)	0.21(3)	0.56(3)	0.95(2)
O1				
x	0.5485(2)	0.5449(2)	0.5437(2)	0.5389 (3)
y	0	0	0	0
z	0.25	0.25	0.25	0.25
Occ.	0.96(1)	0.94(1)	0.92(1)	0.90(1)
B _{iso} (Å ²)	0.43(1)	0.92(4)	1.48(3)	2.24(2)
R-factors				
R _p	2.98	1.97	1.80	1.80
R _{wp}	4.09	2.72	2.44	2.50
R _{exp}	1.83	1.45	1.44	1.43
R _{Bragg}	2.1	2.9	2.80	2.60

Table 2. Refined structural parameters obtained from NPD for $\text{LaNi}_{0.6}\text{Fe}_{0.3}\text{Cr}_{0.1}\text{O}_{3-\delta}$ from room temperature to 900 °C. Space group: $R\bar{3}c$

T (°C)	RT	400	700	900
a (Å)	5.5085 (1)	5.5260 (1)	5.5410 (1)	5.5527 (2)
b (Å)	5.5085 (1)	5.5260 (1)	5.5410 (1)	5.5527 (2)
c (Å)	13.2620 (4)	13.3504 (3)	13.4281 (4)	13.4862 (5)
La				
x	0	0	0	0
y	0	0	0	0
z	0.25	0.25	0.25	0.25
Occ.	1	1	1	1
B _{iso} (Å ²)	0.33(2)	0.59(1)	0.75(2)	0.97(2)
Ni/Fe/Cr				
x	0	0	0	0
y	0	0	0	0
z	0	0	0	0
Occ.	0.63(2)/0.27(2)/0.10(1)	0.63/0.27/0.10	0.63/0.27/0.10	0.63/0.27/0.10
B _{iso}	0.06(2)	0.17(1)	0.22(1)	0.26(2)
O1				
x	0.5542(1)	0.5518(1)	0.5500(1)	0.5483(2)
y	0	0	0	0
z	0.25	0.25	0.25	0.25
Occ.	0.99(1)	0.98(1)	0.97(1)	0.96(1)
B _{iso} (Å ²)	0.56(2)	0.77(1)	0.81(3)	0.97(2)
R-factors				
R _p	3.98	1.76	1.98	2.13
R _{wp}	5.41	2.40	2.64	2.82
R _{exp}	1.78	1.57	1.41	1.41
R _{Bragg}	4.3	3.60	4.70	4.10

References:

- [1] R.H. Mitchell, Perovskites: modern and ancient, Almaz Press Thunder Bay 2002.
- [2] O. Myakush, V. Berezovets, A. Senyshyn, L. Vasylechko, Preparation and crystal structure of new perovskite-type cobaltites $R_1_{x}R_2^{3-x}\text{CoO}_3$, Chemistry of metals and alloys (3) (2010) 184–190.
- [3] M. Retuerto, A.G. Pereira, F.J. Pérez-Alonso, M.A. Peña, J.L.G. Fierro, J.A. Alonso, M.T. Fernández-Díaz, L. Pascual, S. Rojas, Structural effects of LaNiO_3 as electrocatalyst for the oxygen reduction reaction, Applied Catalysis B: Environmental 203 (2017) 363–371.